Īmaka: a Lagrangian Invariant of ELTs.

Olivier Lai*[a], Mark R. Chun[b], John Pazder[c], Jean-Pierre Véran[c],
Laurent Jolissaint[d] , David Andersen[c], Derrick Salmon[a], Jean-Charles Cuillandre[a]
[a] Canda-France-Hawaii Telescope Corp., 65-1238 Mamalahoa Hwy, Kamuela, HI 96743;
[b] Institute for Astronomy, University of Hawaii Hilo, 640 North A'ohoku Place, Hilo, Hawaii 96720;
[c] Hertzberg Institute of Astrophysics, 5071 West Saanich Road, Victoria, BC V9E 2E7, Canada;
[d] AquilaOptics, rue de la Châtellenie, 4, CH-1635 La Tour-de-Trême, Switzerland;
*lai@cfht.hawaii.edu

ABSTRACT

The Īmaka project is a ground layer corrected wide field imager proposed for CFHT. It consists of three processes or components: The dome and local turbulence will be controlled by ventilation; the remaining ground layer turbulence will be corrected by a GLAO system and the free atmosphere seeing will be locally reduced by using an Orthogonal Transfer CCD to correct for tip-tilt within the isokinetic angle of field stars.

In designing the AO system, whether based on an adaptive secondary mirror or using pupil relay optics, it becomes apparent that the conjugation of the deformable mirror is a difficult constraint to achieve given the large field. It turns out this problem is not isolated to Īmaka, because the Lagrange Invariant for our project is in the same range as that of EAGLE for example. The effects of tilting the deformable mirror with respect to the pupil or compensating for misconjugation of an adaptive secondary mirror using a tomographic reconstructor have been investigated using Monte-Carlo simulation codes, including our code developed specifically for GLAO simulations.

We report on quantitative results of performance of Īmaka for a variety of realistic turbulence conditions for each topical scheme, and allude to how these results are applicable to ELTs' adaptive.

Keywords: Ground Layer adaptive optics, deformable mirror conjugation, Monte-Carlo simulations, AO design, atmospheric turbulence.

1. INTRODUCTION

The Canada France Hawaii Telescope, with its 3.6 meter diameter primary mirror, has had a long and successful history of wide field and high angular resolution imaging. There are already many wide field and survey projects planned for the next decade (e.g. HyperSuPrimeCam, Pan-Starrs, LSST), many with larger $A \cdot \Omega$ than could be achieved with the CFHT. However, the site characteristics of Mauna Kea, namely a very thin ground layer, implies that the image quality could be improved over very large fields using the technique of Ground Layer Adaptive Optics (GLAO[1]). Improving the image quality improves the Étendue and improves the overall astrometric accuracy. 8 meter class telescopes are also considering GLAO instruments but the field of view of these telescopes is limited by their optical design to a few to tens arcminutes, providing a natural niche for this older telescope. A facility that is able to take full advantage of the site would produce unprecedented images over large fields of view. Īmaka[2,3] is a path to achieve this on CFHT. Aptly named[†], Īmaka will deliver angular resolutions 2-3 times better than MegaCam enabling new science and also effectively increasing the telescope aperture to compete directly with the 8-10m class telescopes. Īmaka will deliver angular resolutions within a factor of 2-3 of that of the Hubble Space Telescope but with a field of view about 400 times larger than the Advanced Camera for Surveys (ACS). As it turns out, some of the issues raised by the design of a very wide field Adaptive Optics for a small telescope will resurface in classical AO on an ELT due to the fact that the Lagrange Invariant is almost the same for such instruments.

[†] The Hawaiian word Īmaka means a lookout, a scenic viewpoint, and CFHT equipped with this instrument would be an īmaka as this instrument would use the characteristics of Mauna Kea to look at the sky from a special vantage point.

1.1 Ground Layer Adaptive Optics

Selectively correcting the turbulence common to the entire field of interest, namely the turbulence in or close to the pupil of the telescope is a technique known as Ground Layer Adaptive Optics (GLAO). Conceptually, GLAO is a simplified version of MCAO, such that only one deformable mirror is used. The algorithm to determine the optimal wavefront (or correction) to apply to the DM is in theory simpler than MCAO as a simple average will coherently add the parts of the wavefront that are common to the entire field while canceling out the ones that aren't. However, averaging (e.g. Figure 1) is not the most efficient method of retrieving the ground layer turbulence, it needs many guide stars and tomography allows to extract the turbulence common to the entire field as well as the turbulence profile from fewer guide stars; in that sense a linearized tomographic reconstructor can be considered as the optimal GLAO control algorithm.

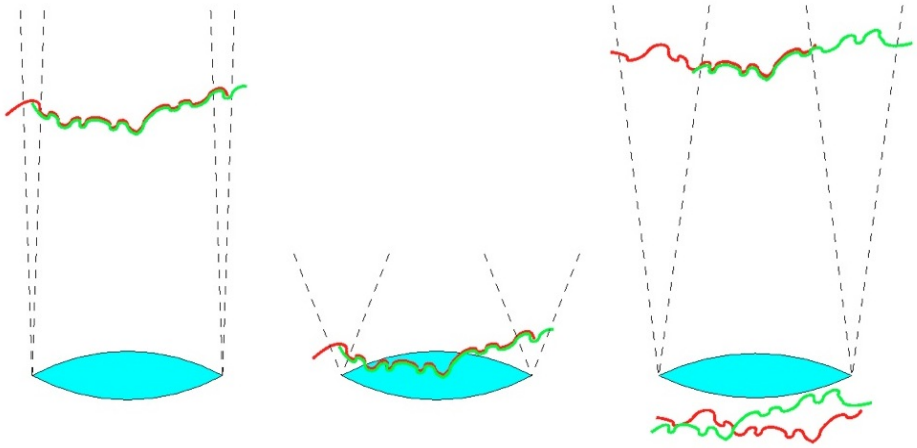

Figure 1: Relationship between altitude of turbulence and corrected field. Left, high turbulence is correlated over small fields only, while lower turbulence (middle) is the same over much larger fields. High altitude turbulence averages out over very large fields, which allows to measure the ground layer turbulence which is common to the entire field.

One important note regarding GLAO correction is that the turbulent phase is only partially (selectively) corrected and thus retains most of the properties of Kolmogorov turbulence, but with reduced amplitude. This has a number of consequences on the type of correction required and the resulting PSF. The ground layer turbulence has to (selectively) be corrected accurately so even though the residual phase error is much larger than conventional AO and the PSF is not diffraction limited, the AO system has to be dimensioned (both spatially and temporally) as if all of the phase at the desired wavelength has to be corrected. Unlike conventional AO, the requirements are somewhat less severe as the performance is asymptotic towards a hard limit, set by the uncorrectable free atmosphere.

1.2 Practical limits of GLAO implementation

The relationship between the corrected field, the thickness of the ground turbulent layer and the achievable image quality is was developed by Tokovinin[1]. It establishes a linear relationship between these parameters based on the geometrical layout of the turblulence with respect to the spatial frequencies that can be corrected:

$$H_{\max} = \frac{\lambda}{\beta \times \theta_0} \tag{1}$$

where λ is the wavelength, β is the goal or achievable image quality, θ_0 is the radius of the corrected field and H_{max} is the maximum altitude corrected in the gray zone. For Īmaka, we turned this around and asked the question, if the maximum altitude to be corrected is 70m, as shown by GLAO site studies[4,5] and the image quality cannot be better than 0.3" due to the free atmosphere seeing, what is the field that can effectively corrected at 700nm? It turns out that θ_0 can be as large as 30' (radius), allowing for a degree field to be corrected.

However, it quickly becomes apparent that when the turbulence is within tens of meters of the pupil, the conjugation of of the deformable mirror becomes much more critical to ensure optimal performance. In fact it is not only the

conjugation of the DM but also the quality of the pupil image. For example in the case of CFHT, the current Cassegrain secondary mirror is conjugated to -40m, making its location unusable for an adaptive secondary mirror. Unfortunately improving the conjugation implies bringing the secondary mirror closer to the primary, making it even larger than the current 1.4m diameter mirror. And conversely, reducing the size of the secondary mirror leads to increased misconjugation. Gregorian designs suffer from the same problem. This led us away from an adaptive secondary mirror solution, as we need very accurate control over the pupil location and quality with respect to the deformable mirror.

Pupil relay

Now in the case of a Cassegrain relay, unless a centro-symmetric design is used (and this comes with its own set of difficulties in terms of vignetting), the deformable mirror will need to be tilted with respect to the plane normal to the optical axis where the pupil is located, if the outgoing beam is to clear the collimating optic of the incoming beam. Because the pupil is laterally de-magnified by a factor *D/d* (*D* is the telescope diameter and *d* is the deformable mirror diameter), the angle of the normal of the DM with the optical axis will magnified longitudinally by $(D/d)^2$. To give an idea of the magnitude of this effect, if a 100mm DM is used on a 3.6m telescope with a 30º tilt with respect to the optical axis to clear the incoming beam collimator, then if one edge of the DM is tangentially in contact with the plane of the pupil, the furthest edge of the DM is 57.7mm; it projects onto the primary mirror with a magnification of $(3.6/0.1)^2 = 1296$, 75 meters above the primary. The angle of the projection of the DM is 87.2º. To correct turbulence that is within tens of meters of the primary, this is a severe problem, especially considering that:

1. Different locations on the DM are conjugated to different altitudes meaning they will project onto different areas of the pupil for different angles, or put differently, different areas of the beam will have different isoplanatic angles depending on how close to the turbulent layers they intersected with the deformable mirror,
2. Different field angles will produce a different apparent stretch of the projection of the DM onto the pupil and,
3. For very large fields, the range of angles of incidence on the DM is such that the geometrical projection of the influence functions will produce a variable corrction as a function of field angles.

If the field of view of the AO system is small, then none of these effects are very important, since although the projection of the DM is stretched with respect to the pupil, it is stretched by a constant, fixed amount which can be taken into account in the calibrations or the interaction matrix. However, the issue now is that the field is so large that the projection of the actuators onto the pupil and turbulent layers (i.e. amount of the stretch) will not be the same for the various field angles (Figure 3). To get an idea of this effect's order of magnitude in conventional terms such as subaperture shift, a 20x20 subaperture system on a 3.6 m aperture with a 1-degree field of view will produce a shift of one full subaperture at an altitude of 10 meters! Clearly, it would be impossible to assign one actuator per area of the pupil if the turbulence is tens of meters thick. The only way to mitigate this problem is make the deformable mirror larger as this allows to reduce the angle of the DM with respect to the pupil and decreases the longitudinal magnification. In fact, Figure 2 shows that to reduce the angle, the DM has to be shifted to the right, and this implies a longer focal length on the collimator, leading to a larger DM.

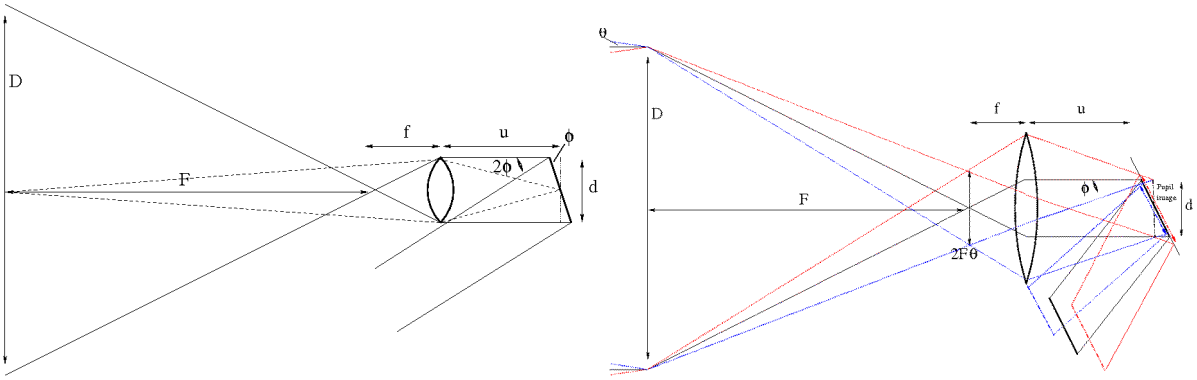

Figure 2: Left, DM tilt angle with respect to pupil necessary to clear incoming beam collimator in case of narrow field. Right, in case of wide field, the collimator has to be larger, proportionally to the field size.

In the case of no (or narrow) field approximation, shown on the left of Figure 2, one can uses the Newtonian form of the thin lens equation $F \times (u - f) = f^2$, along with the facts that $F/D = f/d$ and $d/u = \tan(2\phi)$ to show that the

minimum tilt angle of a DM with respect to the plane of the pupil, θ, for the beam to clear itself from its input collimator is : $\tan(2\phi) = D/(f+F)$ so that:

$$\tan(2\phi) = \left[\frac{D}{F}\left(\frac{d}{D}+1\right)^{-1}\right] \tag{2}$$

Therefore, we see that for narrow field AO systems the DM tilt is usually not a problem, even for relatively large apertures. However, including a field, as shown on Figure 2, right, means that the collimator must be larger than the DM by the physical size of the field plus the blur at the edge of the field at the distance *f* of the collimator. We note that in īmaka, the field of 1° with a focal length *F* of 23m (leading to a proper sampling of 0.1"/pixel at the focal plane with 10μm pixels), the field is approximately 400mm, larger than most conventional DMs and therefore drives the need for larger collimators. In fact, the blur radius is dependent on the pupil magnification, *D/d*; more specifically, the size of the collimator required to collect the light from the entire field is given by - remembering that the DM diameter *d* is still given by $F/D = f/d$:

$$\begin{aligned} &\frac{D/2+F\theta}{F} = \frac{d'/2-F\theta}{f} \\ &d' = d + 2\theta(f+F) = d + 2\theta F\left(\frac{d}{D}+1\right) \end{aligned} \tag{3}$$

where θ is the field half-angle. The exact solution to the minimum DM tilt angle is not trivial but can be approximated by assuming that $\tan(2\phi) = d'/u$, which yields:

$$\tan(2\phi) = \left[\frac{D}{F}\left(\frac{d}{D}+1\right)^{-1} + 2\theta\frac{D}{d}\right] \tag{4}$$

The exact solution requires using the geometrical condition:

$$\tan\left(2\phi - \theta\frac{D}{d}\right) = \frac{(d'-d)/2}{u} \tag{5}$$

which allows to solve for ϕ using the above formulae for *d'* and *u*:

$$\phi = \frac{1}{2}\left[\tan^{-1}\left(\frac{D}{F}\left(\frac{d}{D}+1\right)^{-1} + 2\theta\frac{D}{d}\right)\right] + \theta\frac{D}{d} \tag{6}$$

This approximates the equation above for small field angles. In the case of Īmaka (D=3.6m, F/D=6.5, θ=30'), with a deformable mirror diameters of 100mm, 200mm and 400mm, we find minimum DM tilt angles of 28°, 19° and 12° respectively, values close to the ones determined as providing acceptable vignetting by Zeemax of 30°, 21° and 15° respectively. Extrapolating the necessary DM tilt angle to telescopes much larger than 10 meters produces excessively large angle (>60°) for deformable mirrors smaller than 0.6m for such large fields. In the case of EAGLE, with D=42m, F/D=17.7 and a field of 7.5', the DM tilt angle has to be larger than 32°, 23° and 14° for the above DM sizes, values very similar to those of Īmaka.

Pupil stretch

The reason why this DM angle is so important is that it effectively introduces a pupil stretch with respect to the deformable mirror for different angles, proportional to the DM tilt, as shown on Figure 3, top. Therefore, if we imagine a system with a single turbulent layer right at the pupil, and a tilted DM with the exact on-axis correction applied, as the stretch becomes more important for larger field angle, the residual phase error increases away from the intersection of the DM and the pupil, and the associated PSF increases in width along the perpendicular axis as shown on Figure 3, middle and bottom rows. There is no single shape to apply to the deformable mirror that can satisfy fields beyond a certain separation on the sky. For example, as we saw earlier with a 1-degree field and 20x20 subapertures on a 3.6m

pupil, the two edges of the field will have separated by one full subaperture 10 meters away from the pupil. With a DM tilt of 20 ° and a pupil magnification of 18, the image of the DM will be tilted 81.3° with respect to the pupil. Assuming the intersection of the DM and the pupil is at the center of the pupil, each edge will be 11m away from the primary mirror, effectively shifting the two edges of the field by one full subaperture on the DM. The pupil stretch factor is given by:

$$Stretch = \frac{1}{1 - \tan(\phi)\tan(\theta D/d)} \tag{7}$$

The above example of a 20° DM tilt with D=3.6m, d=0.2m and a one degree field yields a stretch of 1.061 and 0.945 (roughly 5% of the pupil) for the two edges of the field, which is one subaperture for a 20x20 system.

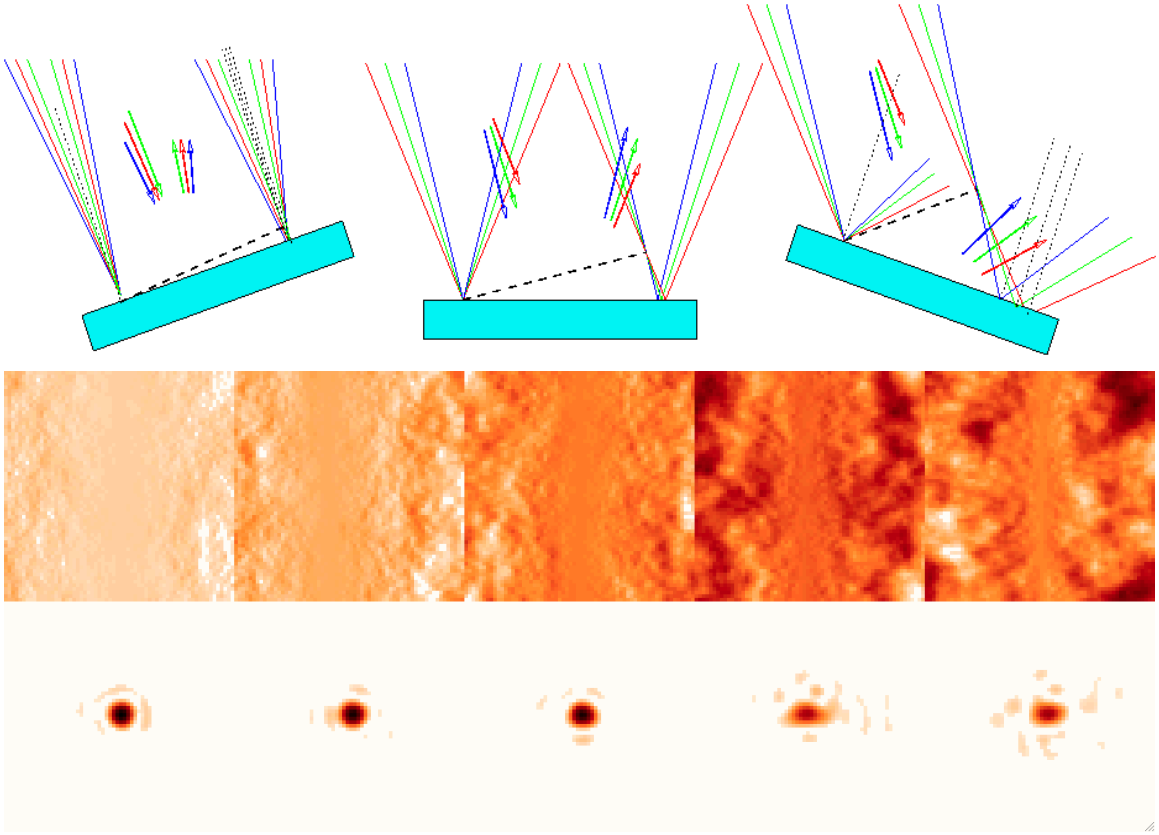

Figure 3: DM tilt introduces stretch of footprint of pupil on the DM for different field angles (top). Subtracting a stretched phase screen from itself (bottom) produces an error that increases away from the optical axis along the direction of the tilt (below); the associated PSFs are increasingly elongated along the direction of the DM tilt.

We note in passing that if the DM is mis-conjugated with respect to the pupil, there is also a magnification of the DM with respect to the beam footprint for each field direction. However, the magnification is not anamorphic as in the case of DM tilt. Therefore, this is less critical because the edges of the field intercept different parts of the mirror and the shape of the DM can be optimized for different field positions, the extreme case of which is MOAO where each field could benefit from correction of a single DM if it was far away enough from the pupil that all the beams' footprints were separated in the meta-pupil.

Influence function projection

A final effect of DM tilt with respect to the pupil is that the influence functions are now projected at an angle to the optical path, and the optical path difference (opd) they introduce has to be multiplied by the cosine of that angle. In fact, the difference in opd is given by a multiplicative factor of $\cos\left(\phi \pm \theta D/d\right) = \cos\phi\cos\theta D/d \pm \sin\phi\sin\theta D/d$. As the opd scaling introduced by the tilt angle of the DM, ϕ, is constant, the correction vector can be normalized by the

appropriate factor, $1/\cos\phi$ and the influence function scaling factor becomes $\cos(\theta D/d) \pm \tan\phi \sin(\theta D/d)$. However, the magnified field angle $\theta D/d$ varies continuously and the same influence function *a*, is seen by all field angles as a different opd due to its projection as shown on Figure 4 (middle right). Assuming that all the turbulence is at the ground and its variance is $1.03D/r_0$ then the residual wavefront due to the influence function projection error will be

$$\sigma^2_{projection} = 1.03(D/r_0)^{\frac{5}{3}} \times \left(1 - \cos(\theta D/d) + \tan\phi \sin(\theta D/d)\right)^2 \quad (8)$$

From this it is possible to compute the Strehl ratio attenuation as a function of Field angle due to the geometric projection of the influence function, taking into account the scaling factor to optimize the image quality on axis (i.e. dividing by $\cos\phi$. Results are shown for the Īmaka case with r_0=0.25m (equivalent to 0.4" for the Ground Layer), at 0.5μm on Figure 11.

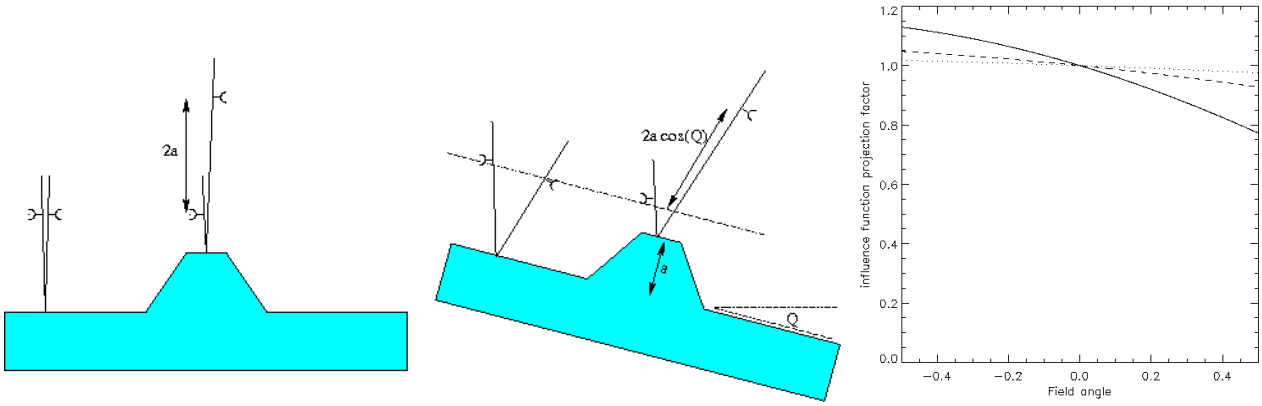

Figure 4: Tilting the deformable mirror with respect to the optical axis introduces a projection of the influence functions. An influence function of height *a* introduces an opd of $-2a\cos(\phi)$ for a tilt angle ϕ. The projection factor and its effect on Strehl ratio is show on the right for $\phi = 30°$, *d*=0.1m (full line), $\phi = 21°$, *d*=0.2m (dashed line) and $\phi = 15°$, *d*=0.4m (dotted line), as a function of field angle θ.

We point out the importance of the product of the field θ and of the pupil magnification *D/d* for all the effects related to DM tilt. Specifically, if we assume that the deformable mirror diameter *d* is fixed by technological constraints, θD will determine the limits of correction for an AO system with an off-axis optical relay. This product is known as the Lagrange Invariant.

1.3 Lagrange Invariant

The Lagrange Invariant, *H*, is a measure of the amount of light propagating through an optical system. From the notation on Figure 2 (right) it is defined as the product of the chief ray angle and the marginal ray height, which is equal to the marginal ray angle multiplied by the chief ray height:

$$H = \frac{D}{F} 2F\theta = \frac{d'}{u} d = 2\theta D \quad (9)$$

We see that this simple formula approximates the formula for DM tilt angle, as $d'/u = 2\theta D/d$. The amount of spatial information is measured by the étendue which is proportional to H^2. As we illustrated above, Īmaka and EAGLE have similar values for their Lagrange Invariant (0.06 Īmaka, 0.09 EAGLE), the Lagrange Invariant also produces design constraints on aspects such as DM tilt. For a constant DM size, the impact of the smaller actuator spacing on DM tilt in an ELT is compounded by the larger pupil magnification. In the above example, we showed that for Īmaka, one full sub-aperture shift occurs 11m away from the pupil for a 1-degree field, with a stretch of 1.06. In the case of EAGLE, if one were to use a 40cm DM to carry the entire 7.5' field, the tilt angle would be 14°, and at the edges of the DM are ±50mm from the plane of the pupil, where the stretch is also approximately 1.06. However with a longitudinal magnification of 11 000x, the edges of the image of the DM are ±550m from the primary mirror and the angle of the DM with respect to

the primary mirror is now 87.5°. We leave it to the interested reader to compute the distance at which a one sub-aperture stretch occurs from the primary mirror.

1.4 The ĪMAKA concept

To take advantage of the site and make ĪMAKA a competitive instrument, a design goal of routinely achieving 0.3" (at 700nm) over a circular degree has been our working assumption. To achieve this, the ĪMAKA concept is composed of three main components: 1) Improvement of telescope environment (dome seeing, telescope infrastructure), 2) the ground layer AO module and 3) the wide field camera.

The location atop Mauna Kea is the best asset for this 4m-class telescope. Realistic modifications and dome ventilation are needed to provide the best natural image quality, comparable to that of the Subaru Telescope. This is obviously a necessary starting point for exquisite image quality of over the entire degree field of view

The Ground Layer AO module, most likely located at the Cassegrain focus, uses a single deformable mirror conjugated to the telescope pupil. Coupled with a relatively high order WFS, it corrects all the turbulence common to the entire field. Over such large fields the probability of finding sufficiently numerous and bright natural guide sources is very high, but a constellation of laser beacons could also be considered to ensure homogeneous and uniform image quality. The image is then limited by the free atmosphere seeing (0.2" to 0.4"). This can then be further improved by an OTCCD camera which can correct some residual high altitude tip-tilt.

The advantages of the OTCCD are not limited to improving the image quality. The PanStarrs1 OTCCD camera is ideal for this project: a simple camera clone would allow to cover one square degree with 0.1" sampling, in perfect accordance with the scientific requirements. The fast read time (6 seconds for 1.3Gpixels) would also lead to the improvement of the dynamic range of the images, all within a reasonable budgetary envelope thanks to the super low cost per pixel of these devices. Finally, the guiding capabilities of the OTCCD will provide the tip-tilt signal if laser beacons are used.

2. SIMULATING ĪMAKA

2.1 Introduction

Although it is possible to understand and get an order of magnitude for the effect of an anamorphic stretch on the correction of an adaptive optics system from the above calculations, this effect is usually neglected in adaptive optics design, and a prescription of a pupil blur smaller than one tenth of a subaperture is the norm. However, in the case of GLAO over such large fields, such a prescription is inapplicable and may even be too strong, as the GLAO correction is only partial in any case. To study this effect in more detail, we developed our own software, especially considering the relative importance of the various error terms in ĪMAKA.

ĪMAKA poses several challenges to simulating its performance. Principally, the field size is about 60 times larger than typical AO fields of view. This leads to enormous memory requirements. ĪMAKA's delivered image quality is also not a diffraction-limited image and averaging of spectral residuals is considerably slower than for a classical AO systems. This plus the fact that many Monte Carle AO simulations include full physical optics wavefront sensing models (e.g. detailed but slow) would require too much computing time to make useful progress. Finally, the ĪMAKA concept is a combination of both GLAO and OTCCD corrections and until recently, no other AO simulation tool was set up to handle a combined yet sequential GLAO and OTCCD correction. These reasons led us to develop a new code, instant_GLAO. While a considerable effort to develop, it was explicitly written to tackle the detailed problems within ĪMAKA, such as DM tilt. Since the Monte-Carlo approach does not lend itself to all type of studies, we also updated the analytic modeling tool PAOLA[6] to be used with ĪMAKA. This allows us to explore quickly general effects (e.g. order of system, variations of the Cn^2 profile, etc.) quickly with PAOLA but also allows us to develop a deeper understanding of how ĪMAKA works with instant_GLAO. We extensively compared all the tools at our disposal and each of these different tools, which each make different assumptions, all yield approximately the same performance.

2.2 Instant_GLAO

The new simulation code instant_GLAO was developed specifically for the study of ĪMAKA. It computes PSFs on a specified grid in a field after correction by a ground-layer adaptive optics system and an Orthogonal-Transfer CCD. Instant_GLAO is a Monte Carlo simulation code based on the geometrical propagation of light through the turbulent atmosphere. The vertical distribution of the turbulence is assumed to be well represented by a discrete set of properly scaled and shifted phase screens. The phase for each field position is computed by summing the appropriate section of

each phase screen. This process is first applied to the direction of the guide stars, and the resulting wavefront measurements are used to compute the shape of the deformable mirror. The residual phase (and associated PSF) is computed by subtracting the DM correcting wavefront from the phase at each PSF field location. A subsequent correction by the OTCCD is to simulate the elastic focal plane of the OTCCD.

The main simplifying assumption of instant_GLAO is that the temporal error (loop lag, closed loop attenuation, etc) can be made small compared to the residual phase error imposed by the free atmosphere. Therefore, to ensure faster convergence, instant_GLAO neglects temporal effects and draws each iteration from a completely uncorrelated random phase shift on each phase screen. This is necessary because unlike classical AO simulations, where every iteration contributes to an improvement of the estimation of the coherent core, in our GLAO simulation each iteration produces wide speckle patterns that take much longer to average out. Also, a consequence of this is that the measurements are made in open loop, as the phase is measured on the guide stars without any prior knowledge of the deformable mirror.

The combined GLAO+OTCCD correction is made at every iteration and normally, for end-to-end run, we consider the atmosphere, dome, mirror figure, and optical design in the aberrated wavefront as well as the conjugation and/or tilt of the deformable mirror. What is notably missing from the current simulations are a more realistic value and power spectrum for the dome seeing including variations with time and the effect of venting the CFHT enclosure, and eventually implementing a WFS model, the temporal bandwidth, and noise.

2.3 Input atmosphere and other phase errors

GLAO over these very large fields of view is very sensitive to the input turbulence profile near the ground. The ratio of ground layer turbulence to free atmosphere turbulence determines the overall maximum gain achievable by GLAO, while the distribution of the local turbulence determines the corrected field of view. As a canonical case, we adopted the "standard" Mauna Kea Turbulence profile near the ground, as measured and reported for the Gemini GLAO study[4] and a limited set of Generalized-SCIDAR data[5] taken at the UH2.2m for the upper atmosphere layers. We note that as a simplification in instant_GLAO, we have moved the upper-most free-atmosphere layer to 3000-meters. The layers are given in terms of their relative strength at a given altitude; a model of the atmosphere is then created by generating as many phase screens as there are layers and normalizing them to a chosen r_0 per layer such that the sum of the phase screens gives the required D/r_0.

To understand the performance under conditions other than the median ground layer and median free atmosphere, we also ran the simulations for the 25% and 75% GL and FA integrated strengths. The ground layer and free atmosphere strengths were found to be uncorrelated[4] so these strengths provide nine (e.g. 3x3) representative cases for the simulations. The dome seeing is obtained from Salmon et al, (2009)[7], which is quoted as 0.43" at 500nm. The dome seeing's main characteristic is its very long correlation times[5]. Since instant_GLAO does not take temporal aspects into account, the way dome seeing is simulated is by adding a Kolmogorov phase screen at zero altitude with r_0=0.24m and L_0=30m. The degradation due to the primary mirror can also be included and we use a phase map estimated by a 64x64 Shack Hartmann obtained in 2004[8]. The primary mirror aberrations are implemented in instant_GLAO by adding this constant phase term to the pupil as shown on Figure 5.

Table 1:Seeing conditions for the nine adopted profiles: Good, median and bad values of seeing (at 500nm) for the nine combinations of 25%, 50%, and 75% ground layer (GL) and free atmosphere (FA).

		Good FA (0.31")	Median FA (0.42")	Bad FA (0.55")
Good GL (0.35")	Total atmospheric seeing	0.503"	0.589"	0.698"
	With dome seeing	0.715"	0.785"	0.877"
Median GL (0.47")	Total atmospheric seeing	0.600"	0.677"	0.778"
	With dome seeing	0.794"	0.860"	0.947"
Bad GL (0.64")	Total atmospheric seeing	0.749"	0.817"	0.906"
	With dome seeing	0.921"	0.981"	1.060"

Lastly, field dependent (chromatic) aberrations due to the optical design can become an important source of error for such large field of view in real systems, especially since the constraints of DM conjugation impose complex solutions to achieve the stringent image quality requirements. These aberrations have been implemented in instant_GLAO, using wavefront phase aberration maps at various field locations exported from the optical design raytrace and interpolated at each location of the required PSFs. These are added whenever end-to-end performance PSFs are computed. Their contribution is usually small but depending on the locations of the guide stars, errors introduced this way can add coherently and propagate as a spurious static aberration.

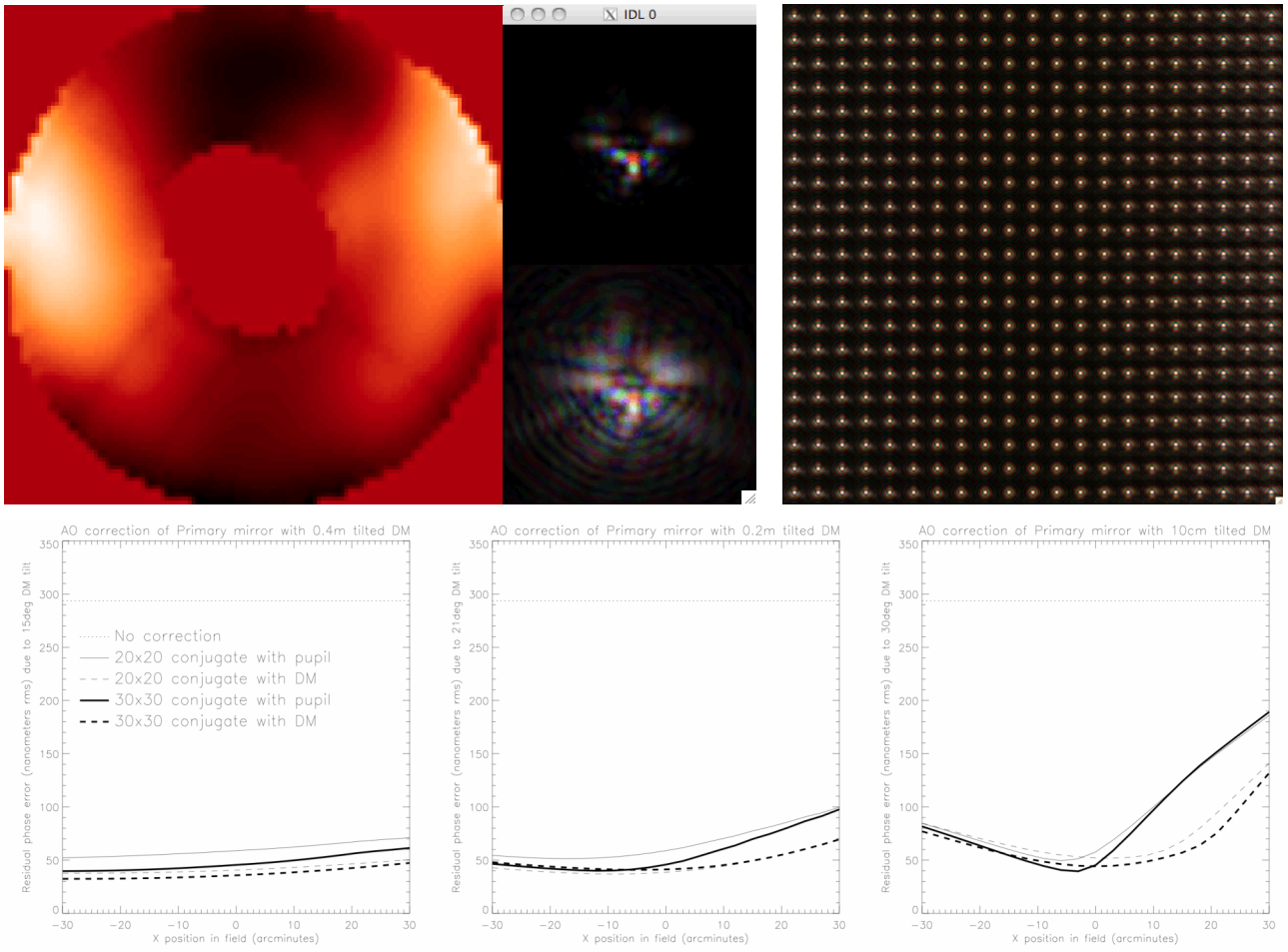

Figure 5: Measured phase map of CFHT's primary mirror (left) and associated PSF (linear and sqrt scale). Right: using a DM with a 30º tilt with respect to the pupil can correct most aberrations on axis, but these 10x10 PSFs over a square degree field show that the correction cannot be adequate everywhere. Bottom panels show the residual phase error as a function of x axis position for 100mm (30), 200mm (21) and 400mm(15) DM for various AO systems.

PSFs without atmospheric deterioration or AO correction were compared to the Zemax model PSFs, and improvements due to AO correction were also studied, as shown on Figure 6. Apart from a very slight improvement at the edges of the field at the shortest wavelengths, using GLAO does not noticeably improve image quality. It might be possible to improve the image quality across the entire field by conjugating the DM to a different altitude, which might be of general interest for MCAO-like techniques, but in our case, the effect is very small especially when compared to the amplitude of residual atmospheric variations. It is also worth noting that the Wynne Dyson design is optimized for a 1° diameter circular field and the PSFs degrade dramatically outside of this area.

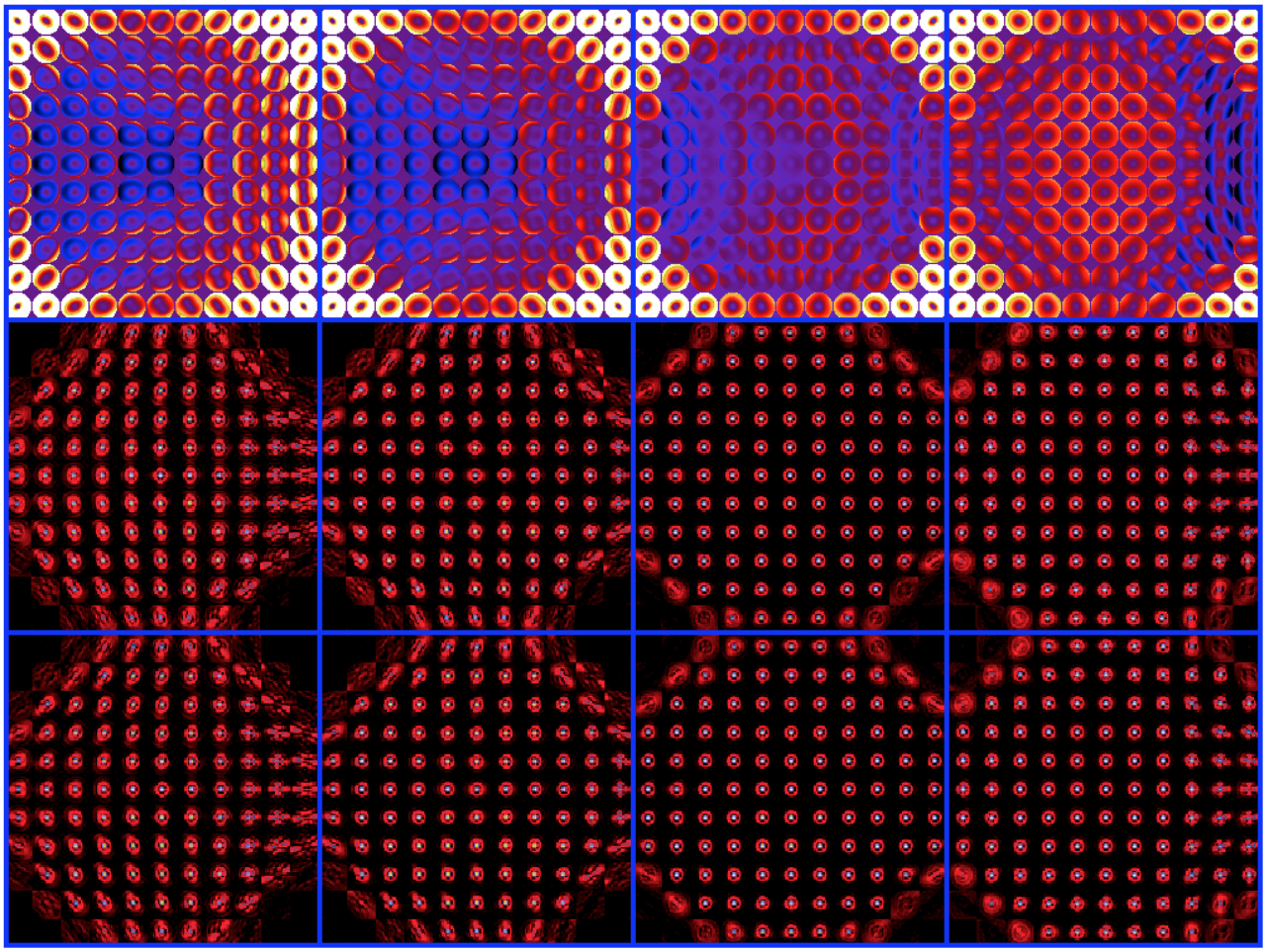

Figure 6: Wynne-Dyson optical design aberrations across the field. 11x11 positions covering 1 degree. Top row: phase, middle row: associated PSFs, bottom row: GLAO corrected PSFs. Left to to right: 450nm, 500nm, 700nm and 900nm. Note that the images central to the field show diffraction-limited FWHM and represent very small contributions ot the overall FWHM of the GLAO system. The dramatic degradation outside the design's field of view is clear.

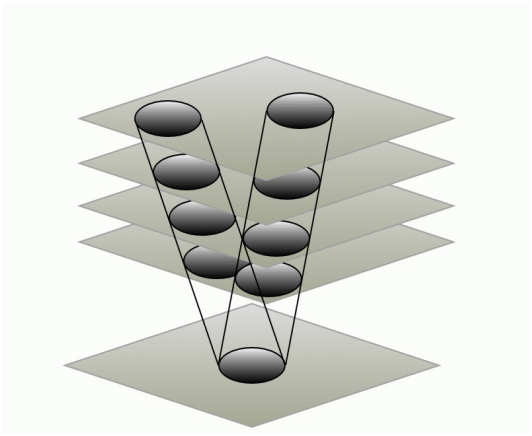

2.4 Algorithm structure

The phase for each field position is computed by geometrically extracting wavefronts from a number of large phase screens preserving the shifts introduced by the different field angles at the different altitudes of the turbulent layers. This maintains the proper correlations and partial corrections of GLAO as shown on the adjacent sketch. This process is first applied to the direction of the guide stars, and the wavefront measurements are used, either by simple averaging or least square minimization of the residual error, to compute the shape of the deformable mirror. The residual phase (and associated PSF) is then computed by subtracting the DM correcting wavefront from the phase at each PSF field location. Measuring the tip-tilt at specified field locations and applying this correction around a specified radius to simulate the focal plane correction of the sub-arrays of the OTCCD then allows simulating the correction brought by the orthogonal transfer..

2.5 Simulation physical parameters

The end-to-end simulations in instant_GLAO include:

- The correction from GLAO and OTCCD within each iteration of the simulation.
- Variation of the number and location of guide stars (both GLAO GS and OTCCD GSs);
- Multiple input turbulence profiles, dome seeing, and primary mirror figure errors (e.g. Figure 5);
- Multiple GLAO wavefront reconstruction algorithms (average phase, zonal, or modal). A tomographic reconstruction is planned.
- Phase error due to tilting or misconjugating the DM (and/or the WFS).
- OTCCD correction (with or without GLAO) using different modes (centroid tracking, average phase, etc) and one-pixel charge shift increments.
- The chromatic field dependent optical aberrations of the telescope and IMAKA optical design (Figure 6).
- Generating PSFs across the entire field of view on a spatial scale less than the isokinetic angle.
- Include g through y-band in wavelengths.
- Zenith angle (see e.g. Figure 7) and
- Resampling of output images to the 0.1" pixels on the OTCCD detectors.

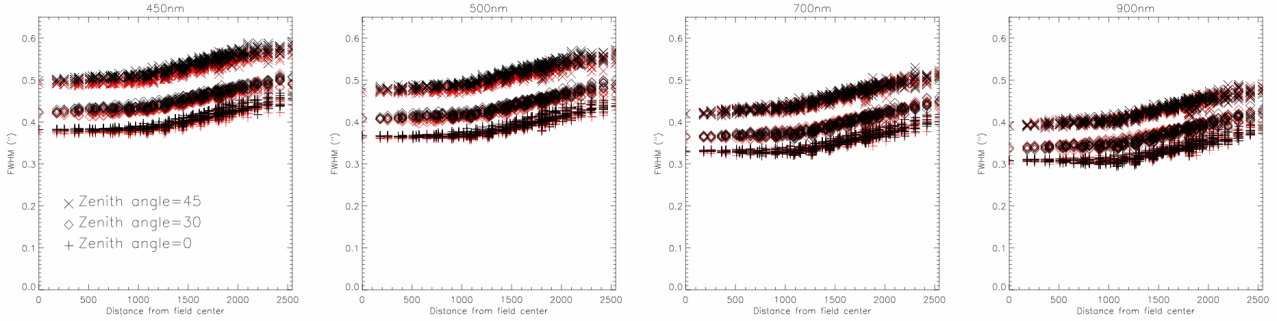

Figure 7: Example of instant_GLAO product, in this case, Zenith angle dependence. red (gray) symbols for a 30x30, black symbols for 20x20. Short wavelengths corrected field is smaller at higher zenith angle.

The basic assumptions and approach followed in instant_GLAO are as follows:

- The major simplifying assumption of this program is that the temporal error (loop lag, closed loop attenuation, etc) can be made small compared the residual uncorrected free atmosphere seeing and can thus be neglected. Therefore, to ensure faster convergence, instant_GLAO neglects temporal effects and draws each new iteration from a completely uncorrelated random phase shift on each phase screen. This is important because in diffraction limited AO simulations, each iteration contributes to estimating the average value of one coherent diffraction core, over an area $(\lambda/D)^2$ while in GLAO simulations the speckle pattern is distributed over $(\lambda/r_0)^2$. A consequence of this is that the measurements are made in open loop, as the phase is measured on the guide stars without any prior knowledge of the deformable mirror.
- Wavefront sensing is achieved by measuring a phase within a subaperture either as the average of all the wavefront sensors, a modal reconstruction of the phase, a zonal reconstruction (à la MCAO), or a tomographic reconstruction (yet to be implemented). We plan on including more realistic forms of wavefront sensors (e.g. Shack-Hartmann, pyramid sensor) in the future but the effects of these measurements are neglected at this point in the development.
- A correction based on the 'sensed' wavefront is applied to the deformable mirror in one of the following ways:
    - The measured average phase is applied as the deformable mirror. This mode is the most basic implementation of GLAO. Its main drawback is that no extrapolation is performed so in cases where the wavefront sensor metapupil (defined by the guide star constellation) is smaller than the DM metapupil (defined by the science field), there can be sharp jumps at the edge of the DM, and this causes the PSF to be broadened by introducing very high spatial frequencies.
    - Zonal control: An interaction matrix is computed at the beginning of the simulation, recording the geometry of the wavefront sensors as a function of the actuators on the deformable mirror. This matrix is then inverted by Singular Value Decomposition, yielding a control matrix that will produce a least

square minimization of the wavefront measurements. This is similar to what an MCAO control system does, in that the geometry of the metapupil is coded in the interaction matrix.
    - A modal control is also implemented, replacing the actuators of the deformable mirror by Zernike modes. These modes are defined on the DM metapupil, so that a basic form of extrapolation can be carried out. However, the performance then becomes quite dependent on the filtering of the inversion.
- DM conjugation/tilt: changing the DM conjugation, either by tilting with respect to or translating it along the optical axis, with respect to the pupil produces a 1-D stretch or 2-D magnification respectively, of the DM with respect to the pupil. The specifics of the DM tilt case are discussed below.
- OTCCD correction: the OTCCD can provide some correction by correcting the local tip-tilt as measured by a nearby tip-tilt star. This tilt may be residual in the GLAO correction or the tilt from the free-atmosphere turbulence. A number of algorithms are possible to generate the tilt correction (nearest neighbor or weighted averages) and a number of approaches can be used to extract the local wavefront tilt (centroid, brightest pixel, phase). In addition, we nominally assume that the OTCCD jitter correction is made in integral pixel shifts on the detector (following current implementations on OTCCD cameras). In the current implementation, the tip-tilt works by measuring the centroid (or the brightest pixel) on the tip-tilt stars, and then applying that shift to all the field locations in the vicinity of this tip-tilt star.
- Atmospheric Cn^2 profile: The highest layer of the free atmosphere of instant_GLAO is at a height of 3000m instead of 12000m to prevent wrapping of the phase screens which would introduce spurious correction of the free atmosphere at certain layers (e.g. for a 0.5 degree field angle, 128 pixels across the pupil and a 1024x1024 phase screen, the phase screen will have wrapped around at an altitude of 3300m). This will have an effect on the OTCCD correction: the isokinetic angle depends on the height and distribution of the free atmosphere layers.

What is notably missing from the current simulation are implementing a wavefront sensor model and including noise, which would allow to study the temporal bandwidth error and the guide star brightness independently. Although we rightfully expect the consequences of including these terms to ever so slightly degrade performance, we also note that the current simulations assume the very worst case of dome venting which is that there is no improvement at all. Better estimates will become available when dome vent models and water tunnel tests are performed. These will be included in the simulation package and should improve performance! instant_GLAO is still being developed and will continue to be used to refine the performance estimation as the estimation of the high resolution C_n^2 profile, the effects of dome venting or the impact of tomographic reconstruction continue to be evaluated of improved.

2.6 Basic system order and comparison to PAOLA

PAOLA (Performance of Adaptive Optics for Large or Little Aperture) is a general purpose AO modeling tool to compute the long exposure AO OTF or PSF in a single shot, including a large number of options and AO modes, continuously developed since 2001 by Laurent Jolissaint (aquilAOptics). This tool has been used for several instrument studies over the past years, and was tested successfully several times against Monte-Carlo codes in all its operational modes, in particular for GLAO. PAOLA makes use of the theoretical relationship between the residual phase spatial frequency power spectrum (PSD) and the long exposure AO OTF, the later being used as an OTF filter applied on the telescope OTF to get the overall telescope+AO OTF. This technique was pioneered by Rigaut et al. (1998)[9] and extended by Jolissaint[7]. As it is an analytic code, a long exposure PSF can be computed quickly with reasonable computing power.

In the context of IMAKA, this code is used to explore the AO parameter space and determine:

- the number of WFS lenslets, in other words the order of the system
- the number of guide stars
- the limiting magnitude and the optimal WFS integration time (FWHM-based)
- the impact of the OTP variations on the PSF
- the PSF structure with GLAO & OTCCD correction

PAOLA was updated specifically for `IMAKA, to be able to deal with large arrays required to cover the dynamic range on the PSD over such large fields and to include the OTCCD correction.

The optimal number of actuators on the deformable mirror or the number of sub-apertures on the wavefront sensor is a trade between delivered image quality, field size/turbulence profile, and sky coverage. The wavefront correction is driven by the shortest wavelengths where the residual wavefront variance has the largest impact on the PSF FWHM but also where the anisoplanatism of the correction is also largest. For larger order systems, the performance at short wavelengths (B, V and even R) is improved with a 20x20 with respect to a 10x10 Shack-Hartmann wavefront sensor (Figure 8, left) and we nominally use 20x20 as our baseline system in instant_GLAO simulations. We therefore make the assumption that using an optimal modal control, or even more appropriately a tomographic optimized reconstructor, can mitigate the loss in performance in the case of fainter guide stars, where a low order system would perform better.

Simulation runs using PAOLA suggest that the GLAO correction from a 20x20 subaperture system can be maintained down to a limiting magnitude of V=14 without degradation to the image FWHM (Figure 8, middle). However, from the point of view of the system performance, there is no such thing as an optimal WFS pitch value that would apply to all conditions. The final choice of the number of corrected modes is a compromise between the image quality, the required sky coverage and the available budget.

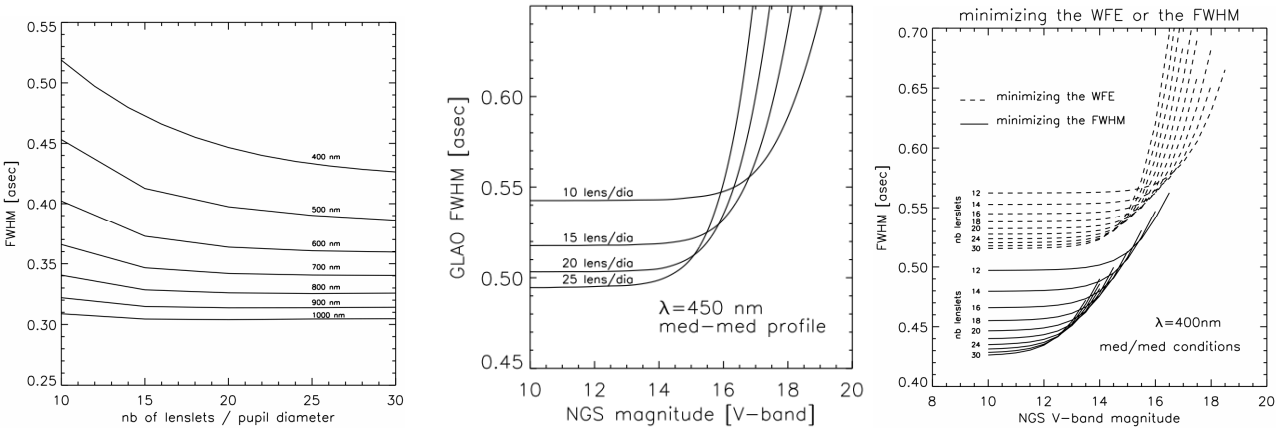

Figure 8: Fitting (left) and photon noise (middle) error as a function of system order obtained by PAOLA (assumed throughput to WFS ~30%). Right: The limiting magnitude is different when minimizing the WFE as opposed to the FWHM; furthermore, minimizing the WFE is not sufficient to minimize the FWHM.

To optimize the system's performance, the WFS integration time and loop gain need to be optimized to minimize the overall noise plus servo-lag error. One would expect that due to the large initial anisoplanatic error, a GLAO system should be less stringent for the overall noise+servo error with respect to a classical AO system and therefore that the limiting magnitude ought to be higher. However this simplified picture is not complete because GLAO doesn't simply reduce the phase variance to below a set level, but rather has to correct a component of the wavefront (high frequencies included) namely the part that is common to the entire field, to a high level of accuracy where its contribution is negligible with respect to the contribution of the free atmosphere. Thus the gain in limiting magnitude is not as large as might initially be expected.

There is another important difference between conventional AO and GLAO that we were not aware of before this study: minimizing the wavefront error is not equivalent to minimizing the FWHM. The best wavefront error does not necessarily lead to the best FWHM, and the difference is quite significant, as shown in the Figure 8 (right). The FWHM difference is about 0.1" at 400 nm. The reason for this is that the PSF wings follow the behavior of the pupil plane spatial frequency phase PSD. In order to minimize the FWHM, the ratio of phase aberrations towards the high frequencies needs to be reduced, and minimizing the phase variance is not necessarily sufficient: high spatial frequencies play a role in broadening the speckle pattern, and yet low spatial frequencies also broaden the speckle pattern by moving this speckle around in the longer exposure image. Therefore there is an optimal balance in the spatial frequencies content required to achieve the lowest FWHM, even at the cost of increasing the overall residual phase error. For example, in the presence of noise, it might be necessary to increase the bandwidth to fully correct the high spatial frequencies; the price to pay is poor SNR on the low frequencies, and this may increase the overall residual variance while providing the best FWHM. Conversely, if the low order aberrations were to dominate the FWHM, it might be necessary to decrease the bandwidth, correct the high frequencies less efficiently and again improve the FWHM. Note that this should be even more pronounced when considering the integrated energy metrics.

3. RESULTS OF DM MISCONJUGATION

While the effects of optical designs, dome seeing, primary mirror aberrations and varying atmospheric turbulence on ĪMAKA's performance have been studied with the help of instant_GLAO, we wish here to focus specifically on the issue of DM tilt because the consequences are more general than the details of a specific instrument, and are applicable to other AO systems where the product of the field and pupil magnification is large.

For a 1-degree field, we simulated DM tilts of 30º, 21º and 15º corresponding to 100mm, 200mm and 400mm DM respectively. One problem arises when the pupil is stretched with respect to the DM and the correction needs to either be extrapolated outside of the WFS metapupil (i.e. the pupil in the case of pupil conjugated WFS). In the worst case of no extrapolation, there are now sharp edges on the residual phase (turbulence – compressed DM), and so we expect one edge of the field to have worse image quality than at the opposite edge where the DM is stretched with respect to the pupil and therefore overfills it.

The results are presented on Figure 9: the FWHM maps (and cuts along x and y axes) show negligible different between the 0 degree (perfect conjugation) case and the 15 degree with a 40cm DM or the 21 degree with 20cm DM case. Only when the tilt angle of the DM with respect to the optical axis gets as large as 30 degrees (allowing a 10cm diameter DM) does the performance degrade noticeably. Note that the results shown are for a wavelength of 700nm, but are relatively achromatic, results at 350nm show much of the same behavior. Also note the asymmetry in performance due to the underfill of the DM with respect to the pupil (right side of the field) when it is compressed rather than stretched.

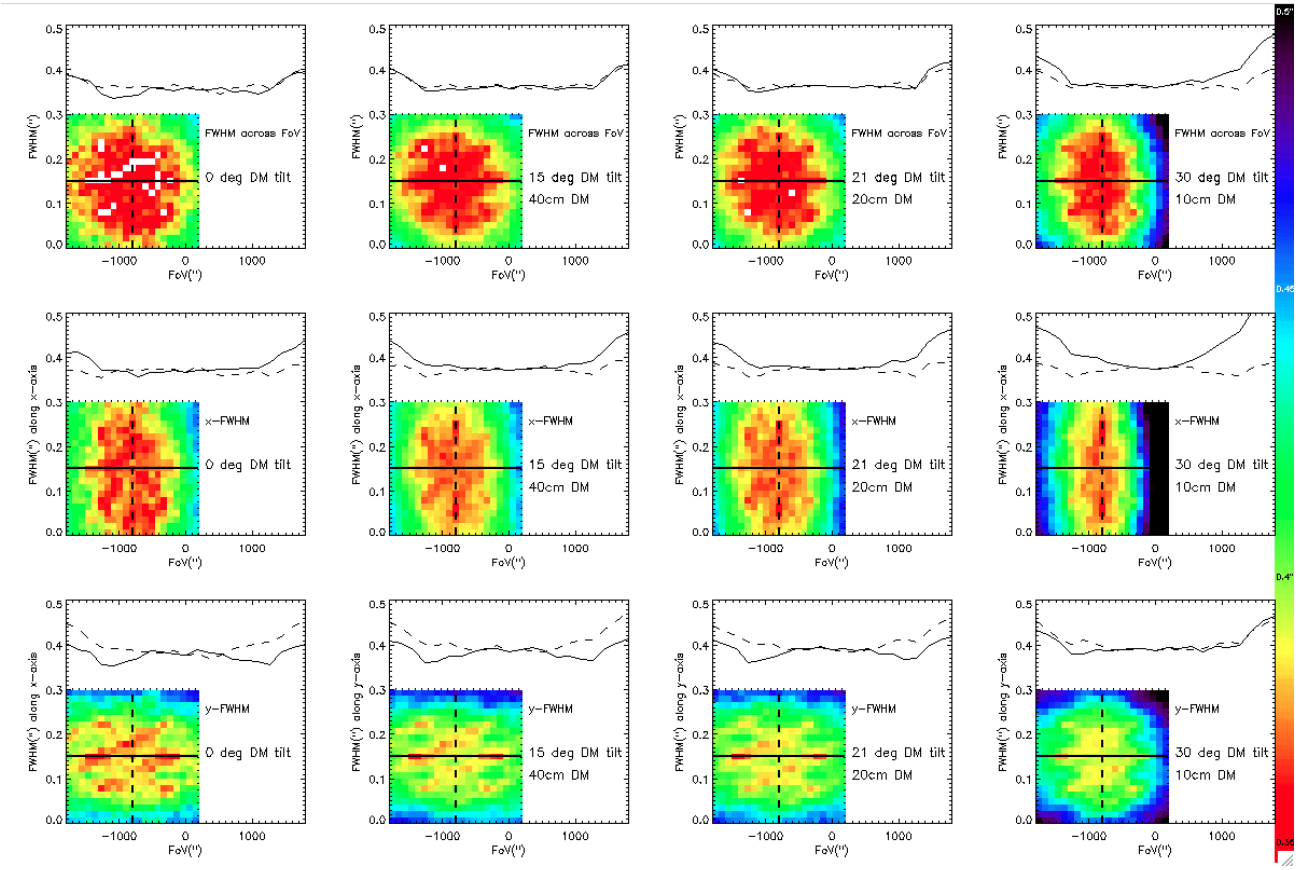

Figure 9: Effect of DM tilt on wide field GLAO performance. Top row, FWHM Gaussian fit, middle row x-FWHM from Gaussian fit, bottom row, y-FWHM from Gaussian fit. Left, no DM tilt, middle left, 15 degrees tilt, 40cmDM, middle right, 21 degrees tilt, 20cm DM, right, 30 degrees tilt, 10cm DM. Each inset, shows a grayscale of the FWHM across the field; print through of 8 NGS is visible, 20' from the center of the field. The effect of DM tilt is very clearly visible on the right edge of the field, especially on the x-FWHM, as expected.

Because parts of the DM contain no information about the wavefront and because the stretch is induced between the measurements and the correction, it appeared interesting to conjugate the WFS with the DM (i.e. tilt the WFS with respect to the pupil so that different field positions illuminate different stretched metapupils on the lenslet array). This kind of correction allows to improve the homogeneity of the correction at the expense of its absolute value. This can be seen on Figure 5 (bottom) and in the figure below:

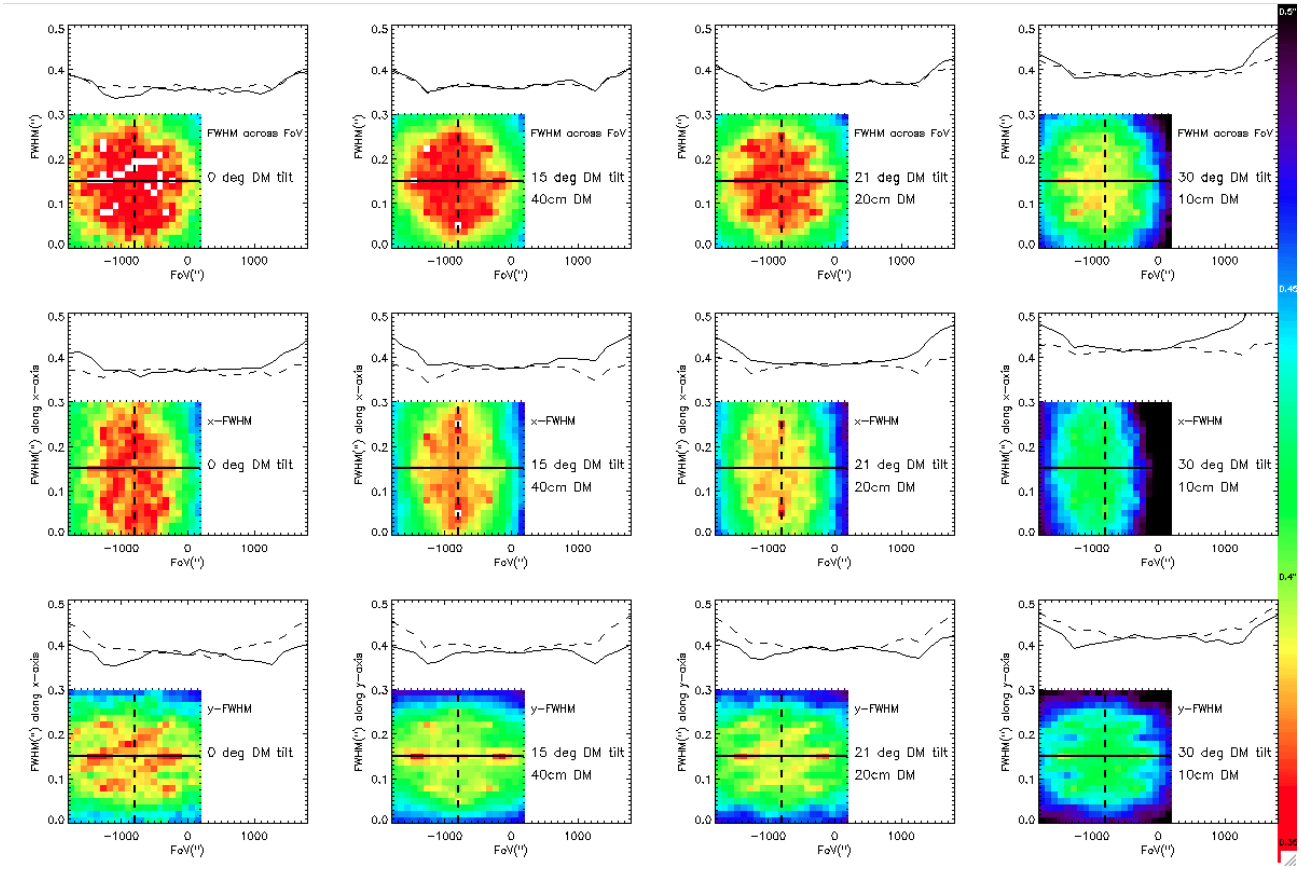

Figure 10: same as Figure 9 but with WFS conjugated to DM. The absolute quality of the correction is degraded but the relative degradation of image quality across the field due to tilting the DM with respect to the pupil is reduced. This is especially visible at the 30 degrees DM tilt (right column) where the effect is most pronounced.

Including the influence function scaling has only a very limited effect for Īmaka, in large parts because the relative degradation of performance is small compared to the absolute residual error due to the free atmosphere as shown in Figure 11 (right). However, looking at the x-FWHM and assuming that the $FWHM \propto a/(S+b)$ (S being the Strehl ratio), we find that by adjusting parmaters a and b to 1.65 and -0.495, there is a very good fit to the model of equation 8 and the data from instant_GLAO simulations as shown by the bold line in Figure 11 . We again note that it is not just the DM tilt angle that introduces the influence function scaling but the product of $\theta D/d$. In the case of an ELT using a MEMs device as a wavferont corrector (i.e. d~10mm), the Strehl attenuation that occurs over a 1-degree field for Īmaka due to influence function projection scaling occurs within 15". Homogeneous image quality over such fields may be difficult to achieve with very small deformable mirrors.

Misconjugating the deformable mirror without any tilt reduces the corrected area, i.e. it increases the variation of FWHM across the field, but it also rapidly decreases the level of performance, as the magnification of the DM with respect to the optical beam for each position in the field means that there is no position in the field for which the DM has exactly the right shape (unlike with mirror tilt, where the on-axis fields have a perfect match between pupil and DM). For `Imaka we found a pretty severe degradation of performance within ±20m of misconjugation. However, since instant_GLAO really only simulates the geometric propagation effects at this point, we found that it was possible to improve the performance by conjugating the WFS to the DM and effectively stitch the metapupil together. As long as

the metapupil at the DM is continouous, the performance can be improved quite dramatically. This result was confirmed by using LAOS[10] to simulate a true tomographic reconstruction of the atmosphere in the code. The performance was more uniform over the FOV and for different DM mis-conjugations: if a tomographic reconstructor is used, it appears that a good GLAO correction can be achieved for this sample atmosphere over a wider range of conjugation altitudes. The GLAO performance only starts to drop when the DM is conjugated to more than 50 m above the ground. Simulations at some DM conjugation altitudes were performed multiple times with different assumptions about the height of the tomographic layers. Results were consistent to 10 to 20 mas. We consider this to be roughly the random error of our modeling and FWHM measurements.

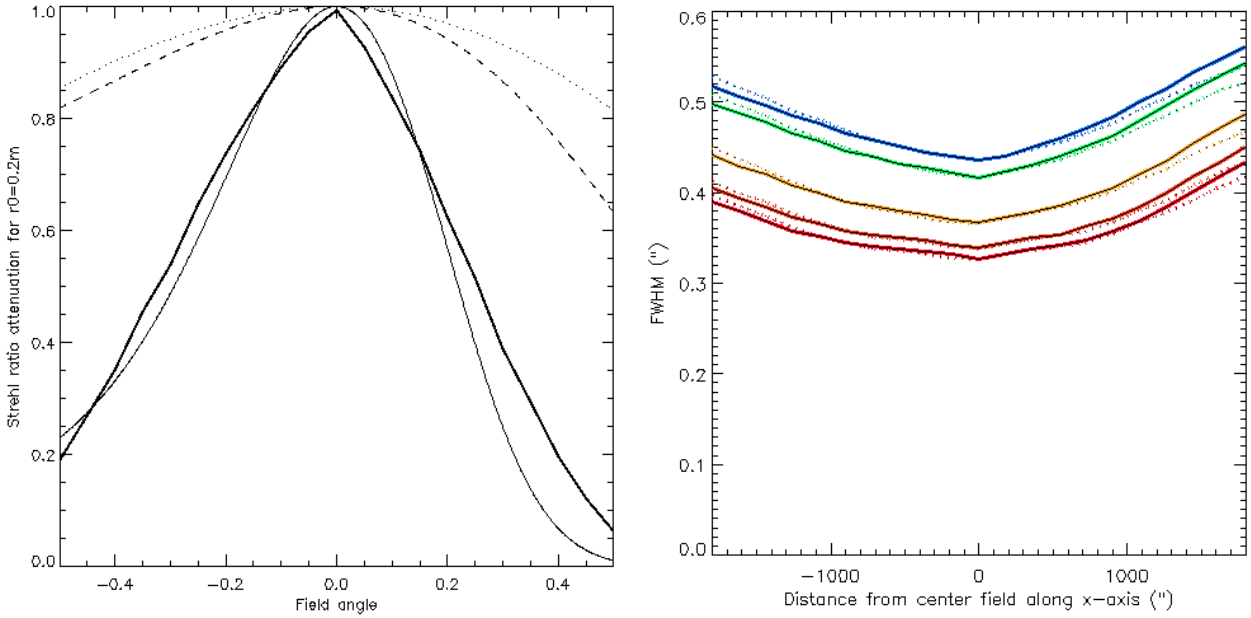

Figure 11. Left: Predicted Strehl attenuation due to influence function scaling for $\phi = 30°$, d=0.1m (full line), $\phi = 21°$, d=0.2m (dashed line) and $\phi = 15°$, d=0.4m (dotted line), as a function of field angle θ and instant_GLAO result (bold). Right: FWHM without (full) and with (dashed) influence function scaling for (from top to botton) 450nm, 500nm, 700nm, 900nm and 1.02μm.

In order to confirm that tomography was responsible for the insensitivity of GLAO performance with DM conjugate altitude, we also ran a version of LAOS that had a GLAO mode in which wavefronts from the six WFS were simply averaged, as in instant_GLAO. For a DM conjugate to the ground, wavefront averaging produced an average GLAO-corrected FWHM within 10 mas of that found from the tomographic simulation. However, for a DM conjugate to 50 m above the ground, the FWHM measured from the wavefront averaging was significantly larger than the FWHM measured from the tomographic simulation. The wavefront averaging LAOS simulations reproduce the same GLAO-corrected FWHM results as the instant_GLAO simulations.

4. `IMAKA PERORMANCE

GLAO only

The first result presented is a representative performance plot of GLAO with the standard Mauna Kea atmospheric turbulence profile. This is the standard test-case, namely a constellation of 8 guide stars on a 20' radius, and the entire field shown is 1 degree. The PSF is computed on a 21x21 grid, every 3' on the field.

The median FWHM values for the inner 40' are 350nm: 0.474", 500nm: 0.423", 700nm: 0.370", 900nm: 0.343". For the inscribed 1 degree diameter field, the median values become: 350nm: 0.483", 500nm: 0.433", 700nm: 0.380", 900nm: 0.350". The values for the full square degree are 350nm: 0.492", 500nm: 0.443", 700nm: 0.390", 900nm: 0.360". The standard deviation due to insufficient phase averaging (1000 iterations) leading to residual speckles is ±3mas at 350nm and increases to ±5mas at 900nm.

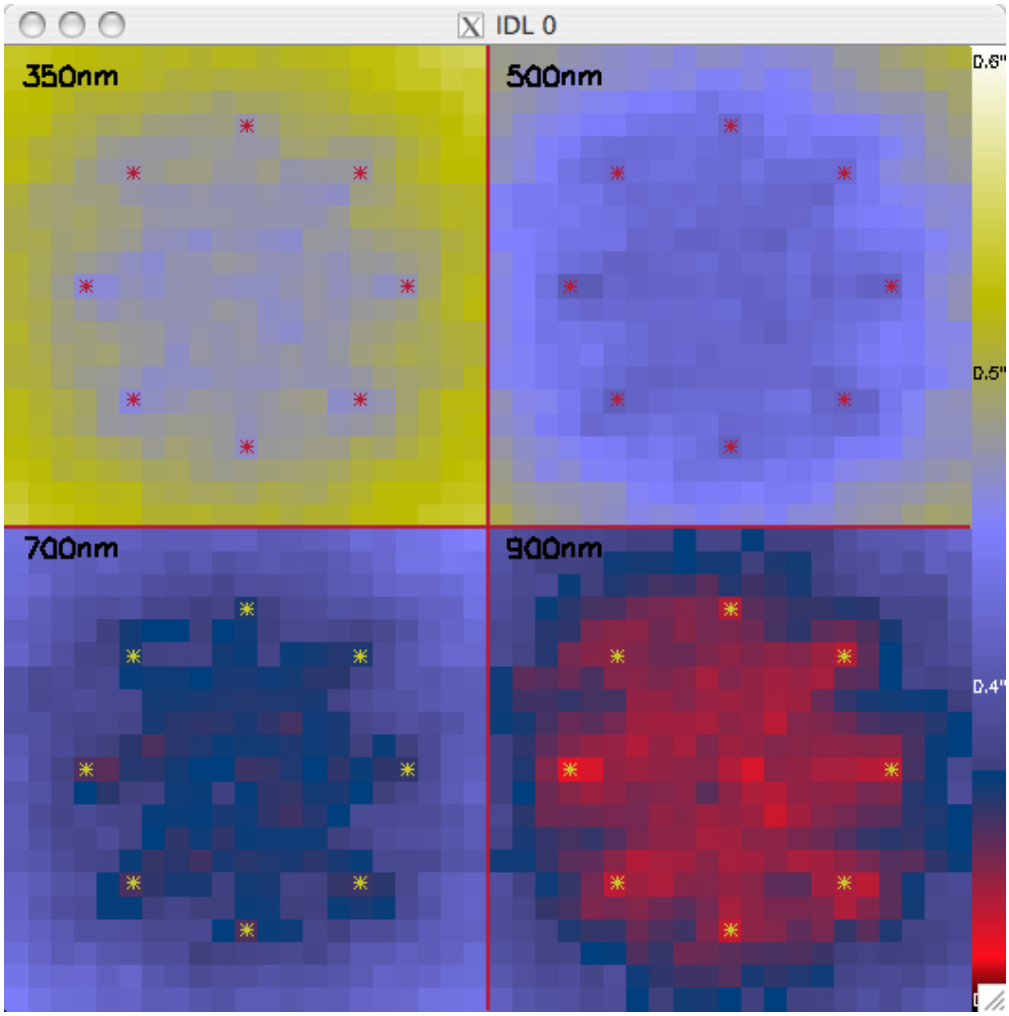

Figure 12: color scale FWHM over 1 degree field of view. 8 guide stars on 20' radius circle. top left: 350nm, to right: 500nm, bottom left: 700nm, bottom right: 900nm.

GLAO+OTCCD

After GLAO correction, the next dominant term in the residual phase error is the uncorrected tip-tilt due to the high altitude free atmosphere. Here the OTCCD can provide some correction by correcting the local tip-tilt as measured by a nearby tip-tilt star.

The tip-tilt works by measuring the centroid (or the brightest pixel) on the tip-tilt stars, and then applying that shift to all the field locations in the vicinity of this tip-tilt star. We have experimented with interpolation schemes in instant_GLAO but because the topmost layer in our simulations is only at 3000m (to avoid wraparound due to the limited size of the phase screens), the isokinetic angle is larger than in reality and we found no noticeable improvement. We have also implemented whole pixel shifts (0.1") for the OTCCD camera, although real systems may be able to transfer only part of the charge.

The simulations are run on a 21x21 field position grid covering the 3600"x3600" field. A test case of 21x21 tip-tilt star was simulated, but with 21x21 field positions, there is not enough resolution to see any anisoplanatic effects: there was a tip-tilt star at every field location where the FWHM was computed these results are therefore a lower limit to achievable resolution across the field. 40' inscribed circular field median FWHM: at 350nm: 0.431", 500nm: 0.372", 700nm: 0.310", 900nm: 0.282". The median values of FWHM for the full square degree are, at 350nm: 0.443", 500nm: 0.384", 700nm: 0.321", 900nm: 0.287". A 7x7 tip-tilt star grid was also simulated (this means there was a tip-tilt star every 10',

or every 3 1/3 field positions). The checkerboard pattern due to isokinetism over such scales is clearly visible in Figure 13.

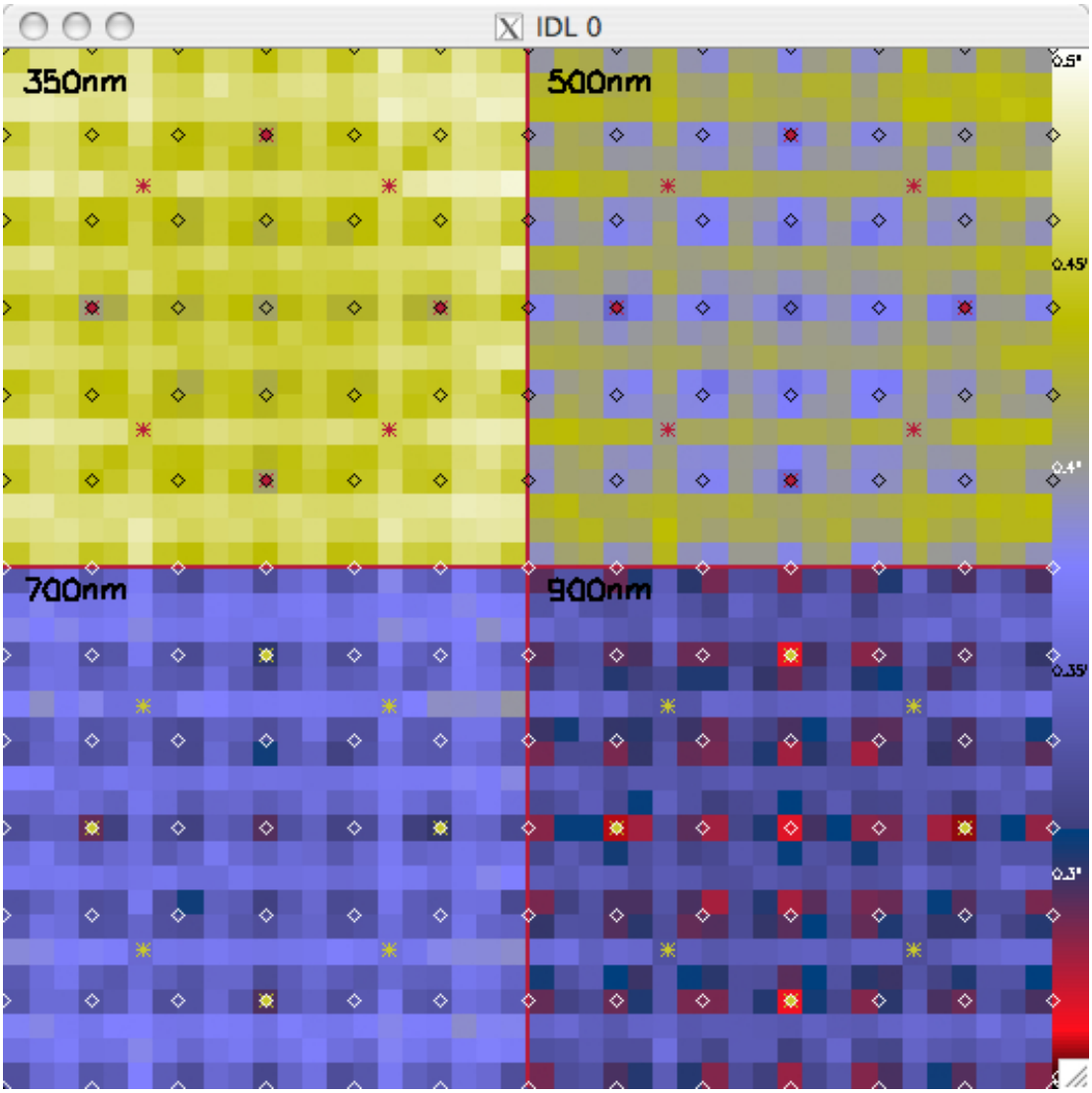

Figure 13: FWHM across 1 degree at 350nm, 500nm, 700nm, 900nm. The stars indicate the position of the 8 GLAO guide stars, the diamonds, those of the 49 tip-tilt stars. Note the different color scale with respect to Figure 12.

The median FWHM values for the inner 40' inscribed circular field are, at 350nm: 0.449", 500nm: 0.401", 700nm:0.352", 900nm:0.327", although median values are not very meaningful in this case.

While most of the simulations made to study the effects of misconjugation used a uniformly distributed asterism of GLAO guide stars, the results presented below were calculated for a constellation of GLAO and OTCCD guide stars taken from a *representative* science field. Here we chose the COSMOS field (http://cosmos.astro.caltech.edu/) due to its importance as a field for extra-galactic studies and its modest galactic latitude (~40 degrees). For this field we found ample guide stars for both GLAO and OTCCD correction within the IMAKA field of view.

For this final perfomance simulations, we included all the realistic effects described above, such as primary mirror aberration, optical design (chromatic and field dependent) aberrations, tilted DM, as well as an extra layer of turbulence at the ground to simulate dome seeing. The performance, as measured by the FWHM, is remarkably uniform over the one degree field of view. For the COSMOS field, eight GLAO guide stars were found near the periphery of the field and

over 130 OTCCD guide stars were found within the one-degree diameter field of view. Figure 12 shows the FWHM derived from an array of 60x60 PSFs (PSFs sampled every one arcminute) across the field. Yellow stars indicate positions of the eight GLAO guide stars while the OTCCD guide star positions are indicated by crosses.

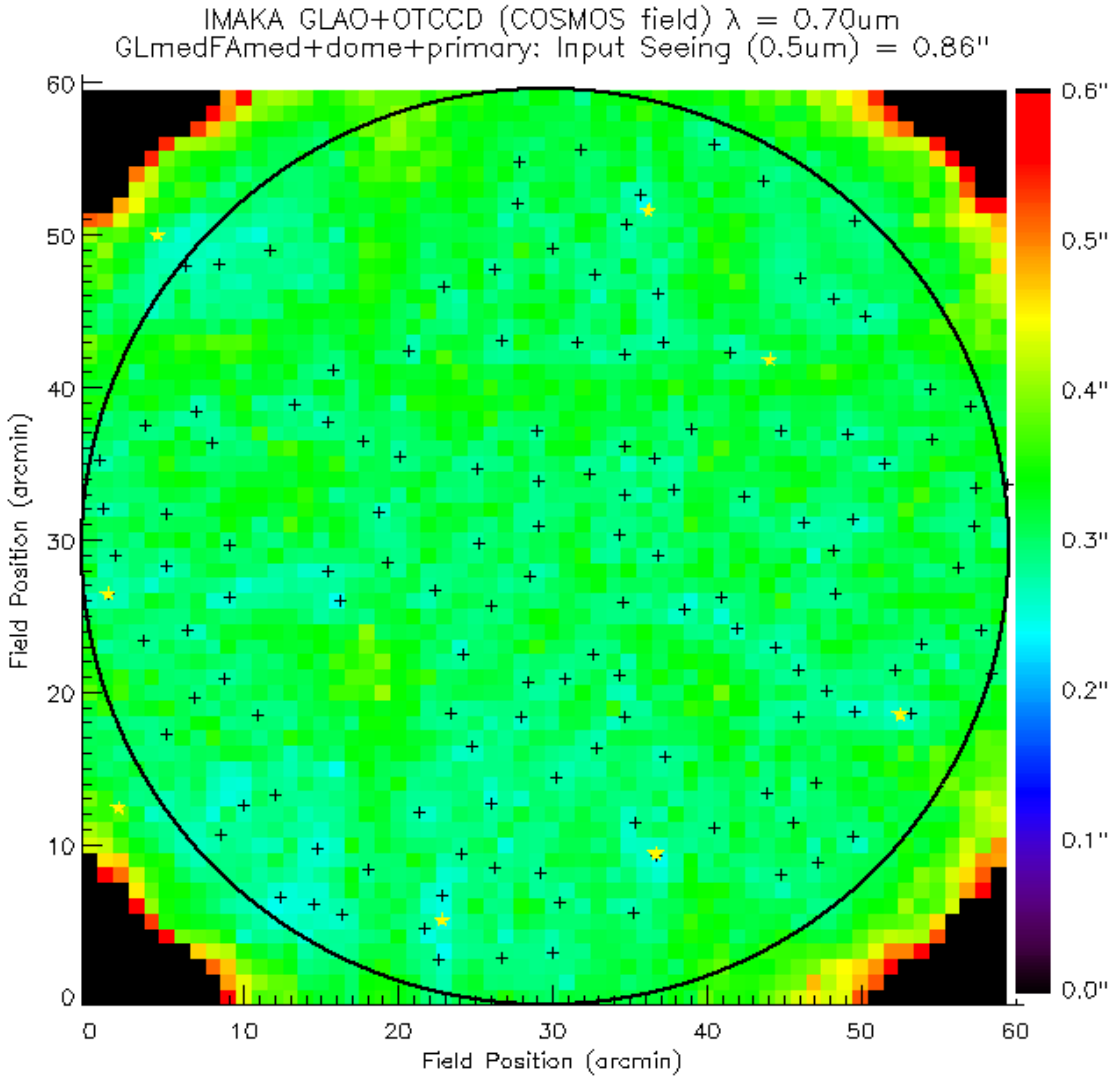

Figure 14:Distribution of FWHM across the one square degree field at an imaging wavelength of 0.7 microns. The one degree diameter field of `IMAKA is shown as well as the positions of the GLAO guide stars (yellow stars) and OTCCD guide stars (crosses)

Our simulations show that median angular resolutions of 0.3" in the visible across a one-degree field of view are thus within reach of CFHT for a GLAO system, taking into account realistic effects such as primary mirror aberrations, optical design aberrations, dome seeing and a tilted DM. We find that an approach using a ground-layer adaptive optics system plus a focal plane detector based on orthogonal-transfer CCDs will deliver superb resolutions under median seeing conditions. Under these conditions, the telescope will have the sensitivity of an 10-m telescope and deliver angular resolutions unmatched over a 1-degree field of view.

5. CONCLUSIONS AND APPLICATIONS TO ELTS

We have presented calculations, simulations tools and results pertaining to the ĪMAKA project for CFHT. We have shown that the tilt of the DM with respect to the pupil is not an insignificant effect both for the optical design and the

performance. We found that a DM of 40cm with a tilt of 15º dot not significantly degrade performance over a full degree field of view, but there is a slight degradation of performance for a 20cm DM tilted 21º, and smaller DMs significantly reduce the corrected field. We have included and studied other realistic effects such as primary mirror aberrations correction across wide fields, and inclusion of chromatic and field-dependent optical design aberration. Even with these stringent design and implementation constraints, this study shows that the IMAKA performance is exceptional for astrophysical applications.

We have also suggested that the issue of DM tilt may be applicable to ELTs through the common Lagrange Invariant between these systems. While ELTs are planning to have adaptive secondary or quaternary mirrors to correct the turbulence common to the entire field – and these will be on-axis – the case is less clear-cut in the case of local correction by a MEMs device as in the case of MOAO. For example, with a standard MEMs device, we can expect a pupil of 10mm which for a 42m entrance pupil, produce a pupil magnification of 4200; a field of 5" requires a DM tilt angle of 8 degrees to clear the collimator, which translates to almost 10 degrees of DM tilt. While this may not appear large, the longitudinal magnification is almost 2.10^6, and the DM angle on the primary is 89.9º. The misconjugation of the MEMs edge (if the center is conjugate to the pupil) are ±14.1km. As long as no vertical resolution of the turbulence is required, then MEMs will not degrade the correction, but any accurate need for conjugation (such as MCAO) will encounter pupil stretch problems. The only solutions are axial designs or larger DMs.

REFERENCES

[1] Tokovinin, A., " Seeing Improvement with Ground-Layer Adaptive Optics," PASP 116, 941-951 (2004).

[2] Lai, O., Chun, M., Cuillandre, J.-C., Carlberg, R., Richer, H., Andersen, D., Pazder, J., Tonry, J., Doyon, R., Thibault, S., Dunlop, J., Pritchet, C., Véran, J.-P., Ftaclas, C., Onaka, P., Hodapp, K.W., McLaren, R.A., Bertin, E., Mellier, Y., Astier, P., Pain, R., " IMAKA: imaging from Mauna KeA with an atmosphere corrected 1 square degree optical imager ," Proc. SPIE 7015, 70154H (2008).

[3] Lai, O., Cuillandre, J.-C., Chun, M.R., Carlberg, R., Richer, H.B., "Imaka:. Imaging from Mauna Kea," Proc. OTAM, 291-298 (2010)

[4] Chun, M., Wilson, R., Avila, R., Butterley, T., Aviles, J.-L., Wier, D., Benigni, S., "Mauna Kea ground-layer characterization campaign," MNRAS 394(3), 1121-1130 (2009)

[5] Butterley, T., Wilson, R.W., Chun, M.,R., Avila, R., Aviles, J.-L., "High Resolution Slodar Measurements on Mauna Kea," Proc. OTAM, 58-65 (2010)

[6] Jolissaint , L., "Analytical Modeling of Adaptive Optics: Foundations of the Phase Spatial Power Spectrum Approach." JOSA(A), 23, 382-394 (2006).

[7] Salmon, D., Cuillandre, J.-C., Barrick, G., Thomas, J., Ho, K., Matsushige, G., Benedict, T., Racine, R., "CFHT Image Quality and the Observing Environment," PASP 121, 905-921 (2009)

[8] Salmon, D., *private communication.*

[9] Rigaut, F.J., Véran J.-P., Lai, O., "Analytical model for Shack-Hartmann-based adaptive optics systems," Proc. SPIE 3353, 1038-1048 (1998)

[10] Gilles, L., Ellerbroek B., Linear Adaptive Optics Simulator v0409; *private communication*.